minerals

MDPI

Article

The Formation of Authigenic Carbonates at a Methane Seep Site in the Northern Part of the Laptev Sea

Alexey Ruban [1,*], Maxim Rudmin [1], Oleg Dudarev [2] and Alexey Mazurov [1]

[1] Division for Geology, Tomsk Polytechnic University, 634050 Tomsk, Russia; rudminma@tpu.ru (M.R.); akm@tpu.ru (A.M.)

[2] V.I. Il'ichev Pacific Oceanological Institute, Far Eastern Branch, Russian Academy of Sciences, 690041 Vladivostok, Russia; dudarev@poi.dvo.ru

* Correspondence: ruban@tpu.ru

Received: 4 August 2020; Accepted: 23 October 2020; Published: 25 October 2020

Abstract: Authigenic carbonates from cold seeps are unique archives for studying environmental conditions, including biogeochemical processes associated with methane-rich fluid migration through the sediment column. The aim of this research was to study major oxide, mineralogical, and stable isotopic compositions of cold-seep authigenic carbonates collected in the northern part of the Laptev Sea. These carbonates are represented by Mg-calcite with an Mg content of 2% to 8%. The $\delta^{13}C$ values range from −27.5‰ to −28.2‰ Vienna Peedee belemnite (VPDB) and indicate that carbonates formed due to anaerobic oxidation of methane, most likely thermogenic in origin. The authigenic pyrite in Mg-calcite is evidence of sulfate reduction during carbonate precipitation. The $\delta^{18}O$ values of carbonates vary from 3.5‰ to 3.8‰ VPDB. The calculated $\delta^{18}O_{fluid}$ values show that pore water temperature for precipitated Mg-calcite was comparable to bottom seawater temperature. The presence of authigenic carbonate in the upper horizons of sediments suggests that the sulfate–methane transition zone is shallowly below the sediment–water interface.

Keywords: authigenic carbonate; cold seep; anaerobic methane oxidation; oxygen and carbon isotopes; fluid source; Laptev Sea

1. Introduction

Methane cold seeps are a widespread phenomenon that occurs on the shelves and continental slopes of inland and marginal seas around the world [1–7], including the arctic seas [8–10]. They represent areas of the seafloor where methane-rich fluids in chemical non-equilibrium with seawater are transported through the sub-seafloor environment and are released at the bottom-sediment–seawater interface [11–13]. The variability of methane seepage activity over time leads to significant changes in sedimentary redox conditions [14,15] and vertical displacement of biogeochemical zones [16,17]. The anaerobic oxidation of methane (AOM) coupled with sulfate reduction (SR) is a key biogeochemical process at seep sites [12,17,18]. AOM and SR are mediated by a consortium of methane-oxidizing archaea (ANME) and sulfate-reducing bacteria (SRB). As a result of AOM, an abundance of dissolved inorganic carbon arises and the alkalinity of pore water increases. The presence of seawater cations (Ca^{2+}, Mg^{2+}) and elevated carbonate alkalinity promote the precipitation of authigenic carbonates [7,19], which show a wide range of mineralogical compositions. The occurrence of Mg-calcite and aragonite in cold seep marine environments has been reported by various authors [1,4,20]. Other carbonate minerals, such as dolomite, ankerite, ikaite, and glendonite, are significantly less common [21,22].

Authigenic carbonates from cold seeps are unique archives for studying environmental conditions, including biogeochemical processes associated with the migration of methane-rich fluid through the sediment column [19,23,24]. The isotopic compositions of carbon and oxygen in authigenic carbonates

are key to solving questions regarding conditions under which carbonates form [25–28]. $\delta^{13}C$ might give information about carbon sources that have participated during carbonate formation (biogenic, abiogenic, or thermogenic methane or their mixture) [29,30]. $\delta^{18}O$ allows for the determination of pore water temperature in which carbonate minerals precipitate [26,31–33].

The present study aims to (1) study mineralogical, chemical, and stable carbon/oxygen isotopic compositions of cold-seep authigenic carbonates collected in the northern part of the Laptev Sea and (2) evaluate the methane source and temperature of fluid involved in carbonate precipitation.

2. Geological Setting

The Laptev Sea is an epicontinental sea with an area of 662,000 km^2. It is bounded by the Taimyr Peninsula and the New Siberian Islands from the west and east, respectively. About 70% of the sea area is represented by a shelf with a depth of no more than 100 m. In 2011, cold seeps were first identified in the northern part of the Laptev Sea (between 76.5–77.5° N and 121–132° E, water depth between 52 and 74 m) during the cruise of R/V (Akademik M.A. Lavrentyev). About 700 individual seeps were recorded using a multi-channel hydro-acoustic complex on an area of approximately 6400 km^2 [34].

The study area is located within the outer shelf of the Laptev Sea, where the Laptev Sea Rift System, the mid-oceanic Gakkel Ridge, and the Khatanga–Lomonosov Fracture Zone are joined [35]. The main structures of the Laptev Sea Rift System (LSRS) are extended grabens and uplifts separating them (horsts) [9]. There are widespread faults represented by northwestern throws and northeastern horizontal faults with a displacement amplitude of up to 2 km [36,37], which can serve as pathways for hydrocarbon migration (Figure 1) [38]. Another factor that could affect the methane migration is submarine permafrost degradation that underlies the shallow part of the Laptev Sea. Methane migration can occur through permafrost taliks that form under flooded thermokarst lakes [39]. The bottom thermal erosion and geothermal heat flow contribute to talik formation. Furthermore, degradation of submarine permafrost can increase methane production in thawed sediments [40].

3. Materials and Methods

3.1. Field Study and Sampling

Bottom sediment samples were collected in and near Laptev Sea's cold seep polygon (Figure 1) during expeditions of RV Akademik M.A. Lavrentyev and RV Akademik Mstislav Keldysh in 2016 and 2018, respectively. The sampling was carried out for bottom sediments in seawater depths of 20–70 m using a boxcorer. The samples were then packed in a polyester sample bag and stored frozen until laboratory analysis. All sampled sediments were dried at 60 °C for 24 h to constant weight. Samples for X-ray diffraction (XRD), X-ray fluorescence (XRF), and stable carbon and oxygen isotope measurements were powdered up to a mean grain size of about 10 μm in a ring mill (ROCKLABS Standard Ring Mill, Dunedin, New Zealand).

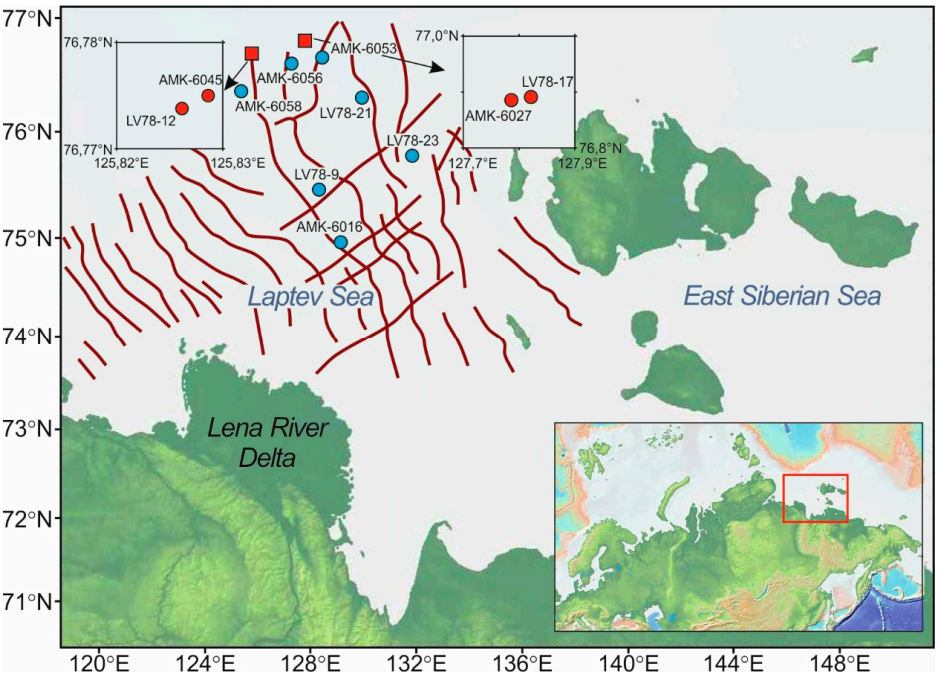

Figure 1. Map showing the locations of the sampling site (the Laptev Sea). The red circle symbol represents stations at which methane seeps were registered. Red lines show the faults of the Laptev Sea Rift System according to Baranov et al. [35] and Sekretov [37].

3.2. Analytical Methods

Grain size distribution was measured using a SALD-2201 laser diffraction particle size analyzer (Shimadzu, Japan). The samples were placed in a mixer bath with distilled water and dispersed using an ultrasonic device (40 W, 40 kHz). Measurements were performed in a flow cell. Grain sizes were classified into three fractions: sand (>63 μm), silt (2–63 μm), and clay (<2 μm).

The bulk mineralogical composition was determined using a Bruker D2 Phase X-ray diffractometer (Billerica, MA, USA) with Cu-Kα radiation at a current of 10 mA and a voltage of 30 kV. Size fractions less than 10 μm of powdered samples were scanned from 5° to 70° 2θ, with a step size of 0.02° and a scanning rate of 2 s. The diverging, scattering, and receiving slits were 1 mm, 3 mm, and 0.3 mm, respectively. Microstructures of carbonates from sediments were studied under a TESCAN VEGA 3 SBU (TESCAN, Brno, Czech Republic) scanning electron microscope (SEM) and an OXFORD X-Max 50 (OXFORD Instruments, High Wycombe, UK) energy-dispersive adapter (EDS) with a 20 kV accelerating voltage, specimen current of 4–12 nA, and a spot diameter of approximately 0.1–2 μm. Carbonate fractions were collected using an optical microscope and fixed to a double-sided 9 mm carbon tab placed on an aluminum stub. It was carbon-coated (30 nm) prior to analysis.

The major element concentrations of the sediments were estimated using a HORIBA XGT 7200 X-ray fluorescence microscope (Kyoto, Japan) operated at a tube current of 0.5, with a 1.2 mm X-ray beam for 100 s and a voltage of 50 kV. The detection limit for major elements was 0.01 wt %. For carbon ($\delta^{13}C$) and oxygen ($\delta^{18}O$) stable isotope analysis, powdered samples of carbonates (approximately 100 μg) were treated with 100% phosphoric acid at 90 °C to release CO_2 for measurements using a Delta V Advantage mass spectrometer (Thermo Fisher Scientific, Bremen, Germany) at the Siberian Research Institute of Geology, Geophysics, and Mineral Resources. The values were expressed using the δ notation relative to the Vienna Peedee belemnite (VPDB) standard for $\delta^{13}C$ and Vienna Standard Mean Ocean Water (VSMOW) for $\delta^{18}O$. The precision of the $\delta^{13}C$ and $\delta^{18}O$ measurements was on the order of 0.1‰. The $\delta^{18}O$ values were converted from VSMOW to VPDB scales using the following conversion [41]:

$$\delta^{18}O_{VPDB} = 0.97002 \cdot \delta^{18}O_{VSMOW} - 29.98 \quad (1)$$

4. Results

4.1. Grain Composition of Sediments

The results of the grain-size analysis for the studied sediment samples show similar particle size distribution. Three size fractions were identified: sand (>63 μm), silt (2–63 μm), and clay (<2 μm). The content of sand, silt, and clay size fractions varied from 0.0% to 5.3%, 65.2% to 89.1%, and 9.6% to 34.9%, respectively, and indicated the predominance of silt among the studied samples. The only exception was station AMK-6056, where sediments were represented by clay silt (the content of the clay size fraction is 34.9%). Sand and clay were not found among the studied samples. The maximum content of the clay size fraction (34.9%) was noted in the sample taken at the AMK-6056 station. The sediments sampled at the cold seep site (stations AMK-6027, AMK-6045, LV78-17, and LV78-12) were represented by dense black silt with a smell of hydrogen sulfide.

4.2. The Bulk Mineral Composition

The bulk mineral composition of the studied samples was represented mainly by quartz, feldspars, and clay minerals (illite + chlorite + montmorillonite; Figure 2a). Small amounts of amphiboles were present, the content of which did not exceed 3% on average (with the exception of sample LV78-23, where their concentration increases to 4.5%). The total content of quartz and feldspars varied between 62.7% to 89.3%, the average being 79.0%. Illite—the content of which ranged from 2.6% to 30.9%—prevailed among clay minerals in all studied samples. In general, the content of clay minerals was within the range of 9.5–37.8%. The maximum content of clay minerals was noted in sample AMK-6056, and the minimum was in the sample from station LV78-23 (depth 22 m).

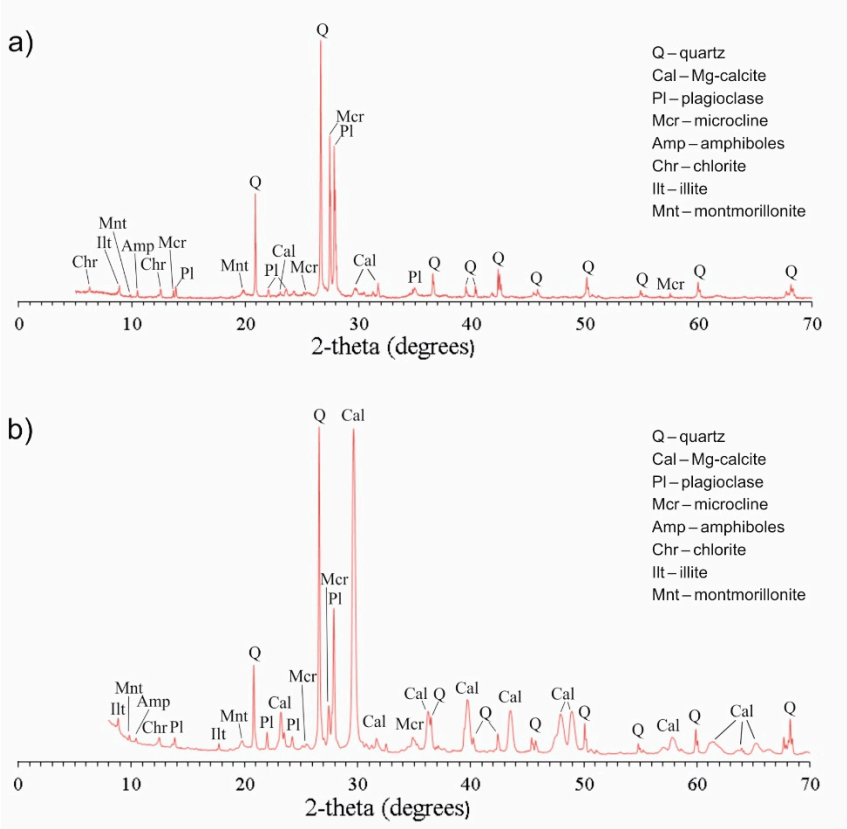

Figure 2. X-ray diffraction (XRD) patterns of host sediments (**a**) and authigenic carbonate nodules (**b**).

4.3. Major Element Composition in Sediments

Major element concentrations in the studied samples are listed in Table 1. Sediments were characterized by the high concentrations of SiO_2 (56.9–65.5%), Al_2O_3 (12.6–14.6%), and Fe_2O_3 (4.2–9.2%), as well as the relatively low contents of CaO (0.9–2.9%). The concentrations of MgO, MnO, P_2O_5, TiO_2, Na_2O, and K_2O were no more than 3%. In general, all studied samples had a relatively homogeneous chemical composition. However, in sediments containing authigenic carbonates, CaO concentrations were significantly higher than non-carbonate sediments.

Table 1. Chemical composition of the studied sediment samples.

Samples	Na_2O	MgO	Al_2O_3	SiO_2	P_2O_5	K_2O	CaO	TiO_2	MnO	Fe_2O_3
AMK-6016	2.9	2.0	14.2	59.0	0.2	2.8	1.9	0.8	0.1	7.5
AMK-6027	2.6	1.6	12.6	61.6	0.1	2.7	1.8	0.7	0.1	5.4
AMK-6045	2.5	2.0	13.4	61.3	0.1	2.9	2.9	0.7	0.1	6.0
AMK-6045/2	2.6	1.8	13.6	61.5	0.1	3.0	2.7	0.7	0.1	6.2
AMK-6053	2.7	2.4	14.6	56.9	0.2	2.9	1.8	1.0	0.1	9.2
AMK-6056	2.4	1.9	14.6	62.6	0.1	2.8	1.0	0.7	0.1	6.5
AMK-6058	2.7	1.8	13.1	61.9	0.2	2.6	1.8	0.7	0.1	6.1
LV78-9	2.9	1.8	14.3	59.7	0.2	2.8	1.7	0.8	0.1	6.9
LV78-12	2.7	1.5	13.8	64.2	0.1	2.5	2.4	0.8	0.1	5.8
LV78-17	2.6	1.3	13.6	65.3	0.1	2.8	0.9	0.5	0.1	4.2
LV78-21	2.3	1.8	13.1	57.9	0.1	2.7	1.9	0.7	0.1	5.6
LV78-23	2.6	1.3	12.7	65.5	0.2	2.1	1.7	0.9	0.1	3.7

4.4. Authigenic Carbonates

Authigenic carbonates were found in three samples collected at stations AMK-6045 and LV78-12. Typical macroscopic features of authigenic carbonate samples are shown in Figure 3. The host sediments were represented by dense black silt with an admixture of clay particles (13.28%). Carbonates were represented by isometric concretions with sizes up to 2 cm in diameter and nodules with a diameter of 2–3 mm (Figures 3 and 4). They have yellow-brown color and a consertal structure and are dense, bioturbated, and strongly cemented in texture. In concretions, we noted cavities up to 4 mm in diameter and hollow channels with a diameter of 1–2 mm.

Figure 3. Photographs of representative cold-seep carbonate nodules collected in the northern part of the Laptev Sea.

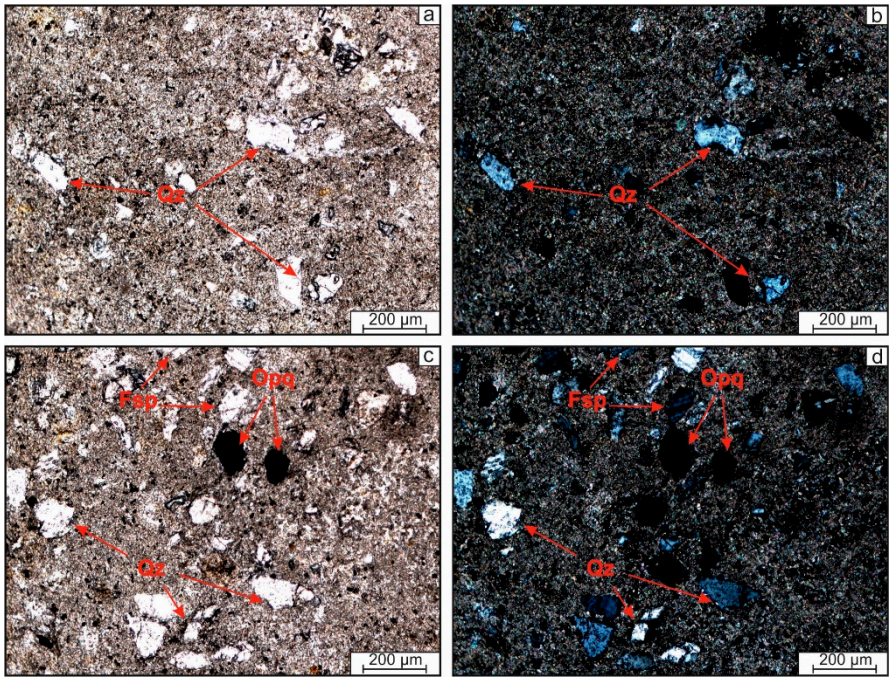

Figure 4. Thin-section photomicrographs in plane- and cross-polarized light of cold-seep carbonate nodules (sample AMK-6045/2): (**a**,**b**) typical carbonate matrix; (**c**,**d**) detrital grains of quartz, feldspars, and opaque minerals are interspersed within carbonate matrix. Qz—quartz, Fsp—feldspar, Opq—opaque minerals.

Petrographic observations show that the carbonate concretions are made up of a homogeneous microcrystalline carbonate matrix (Figure 5a), in which detrital grains of quartz, feldspars, and opaque minerals, are interpsersed (Figures 4 and 5c,d). The XRD analysis of the carbonate nodules (Figure 2b) revealed that the carbonate phase is represented by Mg-calcite (25–36%). The accessory non-carbonate minerals were mainly quartz (22–28%), feldspar (23–29%), clay minerals (illite + chlorite + montmorillonite, 18–23%), amphiboles (~1%), and halite (~1%). Quartz and feldspars were represented by semi-rounded silt-sized grains randomly scattered within the carbonate matrix (Figures 4 and 5d). The results of the EDS analysis show that the Mg content in calcite varied from 2% to 8%.

Authigenic pyrite was found in samples AMK-6045, AMK-6045/2, and LV78-12, and was in paragenesis with Mg-calcite (Figure 5b,e). Moreover, it was the main form of iron disulfide in carbonate concretions. Pyrite was represented by individual microcrystals in cubic and occasionally octahedral forms embedded into Mg-calcite nodules. The size of pyrite crystals varied from 2 to 10 µm. Sample LV78-12 contained individual pyrite framboids no more than 5 µm in size that were adsorbed on the surface of clay minerals.

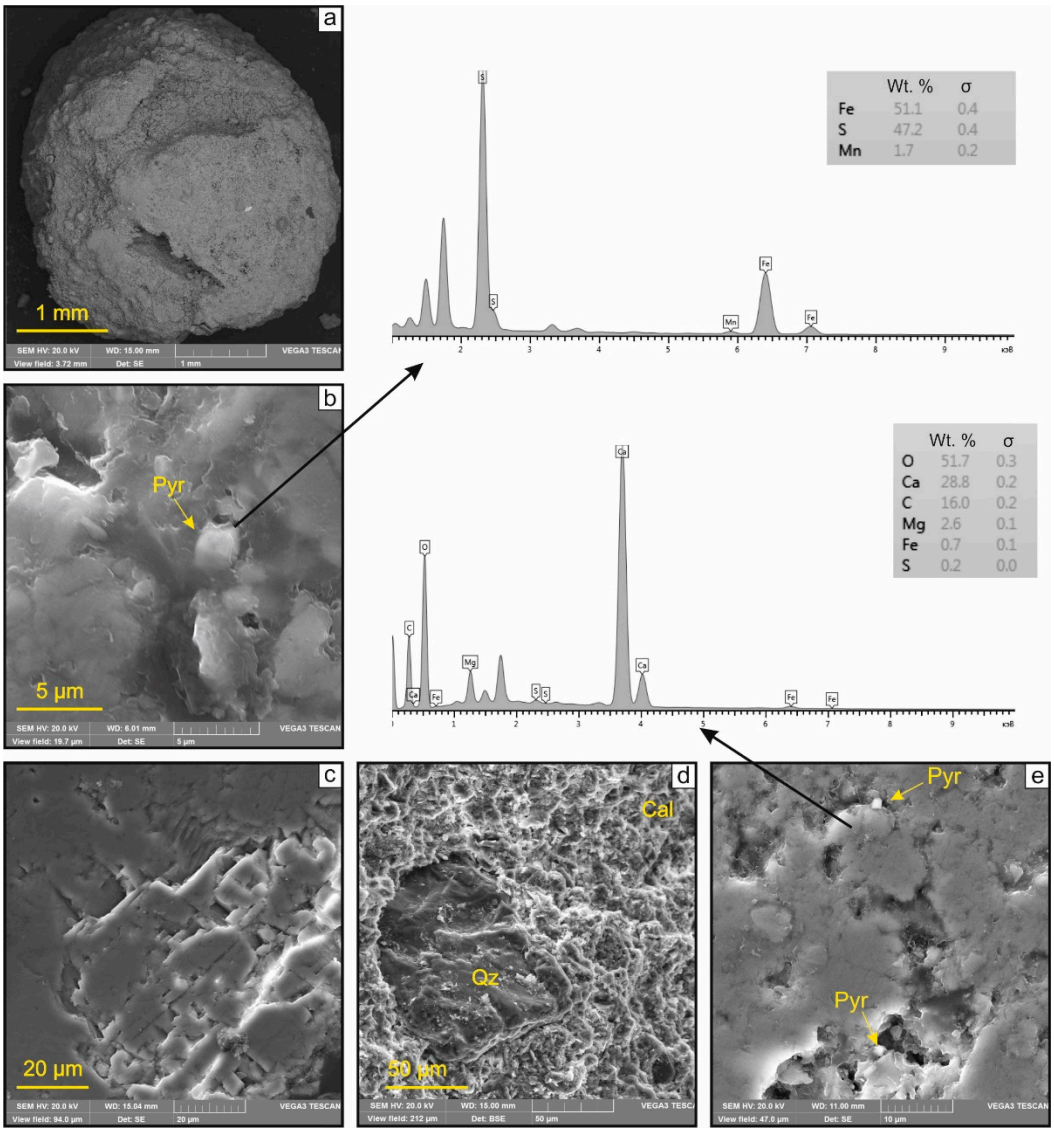

Figure 5. Scanning electron microscope (SEM) images illustrating the morphology and internal structure of authigenic carbonates: (**a**) nodule of Mg-calcite (sample AMK-6045); (**b**,**e**) euhedral pyrite in Mg-calcite matrix (sample LV78-12); (**c**) microcrystalline structure of Mg-calcite (sample LV78-12); (**d**) quartz fragments in Mg-calcite matrix (sample AMK-6045/2). Qz—quartz, Cal—Mg-calcite, Pyr—pyrite.

4.5. Stable Carbon and Oxygen Isotope Data

The collected carbonate samples had very similar carbon- and oxygen-stable isotopic compositions. All samples had negative $\delta^{13}C$ values and positive $\delta^{18}O$ values. The $\delta^{13}C$ values ranged from −27.5‰ to −28.2‰ VPDB (mean = −27.7‰ VPDB). The $\delta^{18}O$ values varied from 3.5‰ to 3.8‰ VPDB (mean = 3.6‰ VPDB; Figure 6).

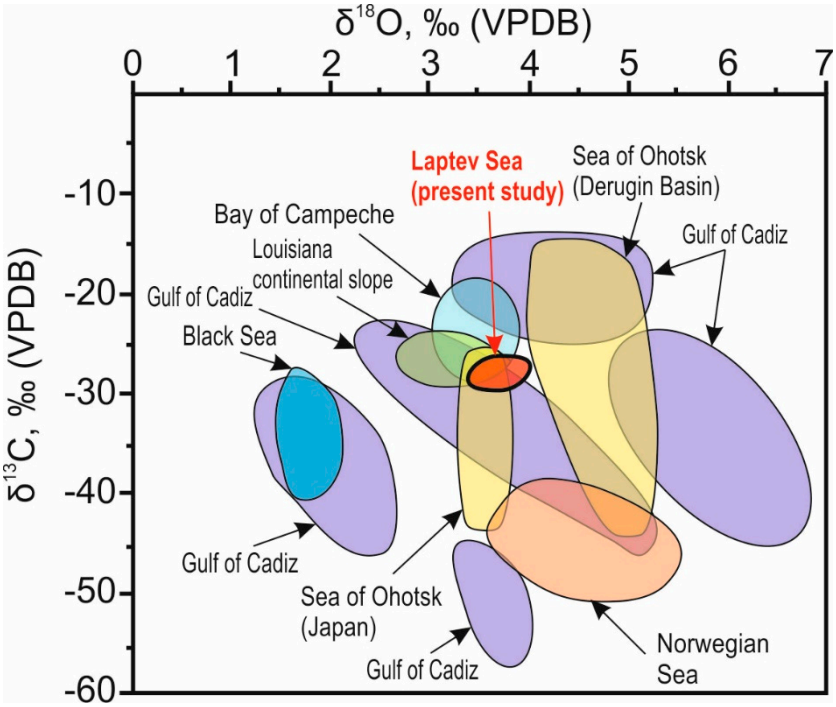

Figure 6. Carbon and oxygen isotopic compositions for authigenic carbonates from the Laptev Sea in comparison with other authigenic carbonates from different areas. Isotopic data for carbonates from Sea of Ohotsk, Norwegian Sea, Black Sea, Louisiana continental slope, Bay of Campeche modified from [26] and references therein, and for carbonate chimney samples from the Gulf of Cadiz modified from [42,43].

5. Discussion

Petrological, mineralogical, and isotope geochemical characteristics of the authigenic carbonates provide important information for understanding their formation mechanisms as well as the source and temperature of fluids.

Recent investigations of sediment grain size in the study area [44,45] have shown that the main type of surface sediments was silt and clay. However, in some sites of the study area, poorly sorted sediments composed of multiple grain sizes (including grain >1 mm) were found. Methane seepage, which can contribute to the "washout" of the clay and silt size fractions has been proposed as one of the hypotheses that explain such a distribution of grain size in the sediment. The results of the grain size analysis obtained in this study show a rather uniform grain size composition of sediments and practically the absence of the sand fraction. The grain size, as well as the bulk mineral composition, of the host sediments from the studied cold seep sites and background sediments are very similar.

A distinctive feature of modern bottom sediments of the Arctic seas, as compared to the sediments of the seas of humid and arid zones, is the almost complete absence of carbonate minerals in their composition. The reason for this is the increased solubility of CO2 caused by low seawater temperatures [46].

Among the studied samples, authigenic carbonate, represented by Mg-calcite, was found in samples AMK-6045, AMK-6045/2, and LV78-12. The dissolved methane concentrations in the surface seawater and hydroacoustic data confirm active methane seepage at the site where these samples were collected [9,34,47,48]. Mg-calcite-associated pyrite indicates the activity of the sulfate reduction process during carbonate precipitation in an anaerobic environment [24,49]. Pyrite formation probably occurred during the interaction of hydrogen sulfide produced due to sulfate reduction with iron ions (the source of which is detrital minerals). As a result of this reaction, metastable iron monosulfides (mackinawite, greigite) were formed, which subsequently recrystallized to pyrite [6,50].

The presence of carbonate and sulfide authigenic minerals in the upper horizon of sediments (~5 cm) suggests the shallow position of the sulfate–methane transit zone [51,52]. AOM often occurs in the upper horizon of sediments or even directly at the sediment–seawater interface at high fluid flows [53–55]. In this case, the pore waters should be characterized by high concentrations of sulfate ions, which would cause aragonite precipitation [4,49]. However, Mg-calcite was the only form of calcium carbonate in the studied samples. In addition to SEM and XRD results, the Mg/Ca ratio in the host sediments confirms this [56,57]. The Mg-calcite precipitation probably occurred in a reducing environment with a sulfate depletion in pore water and the participation of dissolved sulfide, as was shown by the example of carbonates from the Arabian Sea [58]. These geochemical conditions differ from that of hydrocarbon seeps in the Gulf of Cadiz [42,59,60], where pyrite forms in the association with carbonates and Fe-Mn nodules [61].

The isotopic composition of carbonates can often show effects of mixing of carbon from different sources (hydrocarbon gases including methane, crude oil, dissolved carbon in seawater, marine biogenic carbonate, and organic sediment matter), which makes it more difficult to identify the composition of the parent carbon [32,42,43]. An example of mixing methane sources has been reported for hydrocarbon-derived carbonate chimneys in the Gulf of Cadiz [42,43]. The carbon isotope composition of authigenic carbonates from stations AMK-6045 and LV78-12 was characterized by a very small variation of the $\delta^{13}C$ values (Figure 6). The narrow range variation of the $\delta^{13}C$ (from −27.5‰ to −28.2‰) values indicate the predominance of a single carbon source during the precipitation of these authigenic carbonates. Moreover, the $\delta^{13}C$ values suggest that the carbonates formed due to anaerobic oxidation of ^{13}C-depleted methane [4,13,32,62].

Typically, seep carbonates have higher ^{13}C values than the parent methane due to the incorporation of carbon from sources other than methane [34,63–65]. For example, isotopic values of biogenic (microbial) methane vary from −50‰ to −110‰, while carbonates that formed from this methane type typically have $\delta^{13}C$ values ranging from −40‰ to −60‰ [13,30,32,42]. Furthermore, microbial activity during AOM has a fractionation effect for $\delta^{13}C$, consequentially offsetting δ13C methane by approximately 20‰ to 60‰ [1,66].

The negative carbon isotope compositions of studied carbonates samples (average −27.7‰) indicate that the most likely carbon source is thermogenic methane ($\delta^{13}C$ values of thermogenic methane range from −30‰ to −50‰ [42,67]). Carbonates derived from this methane type have $\delta^{13}C$ values varying from −20‰ to −50‰ [42,68,69]. The source of thermogenic methane is likely to be gas condensate or oil reservoir in underlying sedimentary sequences. The molecular composition of sediment organic matter in the study area suggests hydrocarbon migration from underlying deposits [70]. Faults of the Laptev Sea Rift System can serve as pathways for upward migration of methane. Gas hydrate deposits, which hypothetically accumulate under submarine permafrost [34,39,48] can also be a potential source of thermogenic methane. It should be noted that carbonates resulting from oxidation of crude oil have $\delta^{13}C$ values ranging from −25‰ to −30‰ [71], but in this case, they showed spots of biodegraded crude oil within the carbonate samples [26,72–74]. In our case, oil spots were not observed. The contribution of sedimentary organic matter was not considered because the total organic carbon content in the sediments collected at or near the sites where the carbonates were recovered did not exceed 1% [45].

The oxygen isotope composition of the authigenic carbonates provides additional information on the seawater/pore water temperature during precipitation and the $\delta^{18}O$ values of the pore-fluid from which the carbonates precipitated [26,64,65,75]. In this research paper, the theoretical values of $\delta^{18}O_{fluid}$ were calculated using the bottom seawater temperatures, using the equation proposed by Anderson and Arthur [75]. The average temperature of the bottom seawater at the stations where carbonates were sampled was about −1.5 °C (unpublished data). The calculated $\delta^{18}O_{fluid}$ values range from −0.5‰ to −0.2‰ VSMOW and were comparable to the $\delta^{18}O$ values of the bottom seawater in the northern part of the Laptev Sea (from −0.7‰ to 0.4‰VSMOW; [76]). Assuming that $\delta^{18}O_{fluid}$ was

in equilibrium with $\delta^{18}O_{seawater}$, the authigenic carbonates of the present study precipitated under the same pore water temperature as the bottom water temperature.

6. Conclusions

In this study, we characterized the major oxide, mineralogical, and stable isotopic compositions of authigenic carbonates from methane seep site of the northern part of the Laptev Sea. These carbonates were represented by Mg-calcite with a magnesium content between 2% to 8%. The negative carbon isotope compositions of studied carbonate samples suggest that carbonate formation was a result of the anaerobic oxidation of thermogenic methane (average carbonate $\delta^{13}C$ −27.7‰). Authigenic pyrite within the carbonate matrix is evidence of sulfate reduction during anaerobic oxidation of methane. The hydrogen sulfide produced in this process interacted with the iron ions contained in pore water, resulting in precipitation of iron monosulfides, which recrystallized into pyrite. The narrow range of the $\delta^{13}C$ values indicates the predominance of a single carbon source during the precipitation of these authigenic carbonates, which was probably thermogenic methane. The calculated $\delta^{18}O$fluid values show that pore water temperature during Mg-calcite precipitation was comparable to bottom seawater temperature. The presence of authigenic carbonate in the upper horizons of sediments suggests that the sulfate–methane transition zone is located shallowly below the sediment–water interface.

Author Contributions: A.R. conceived and designed the study; A.R. and M.R. performed the laboratory investigations; A.R., M.R., O.D., and A.M. analyzed the data; A.R. and O.D. contributed materials; A.R. wrote the paper. All authors have read and agreed to the published version of the manuscript.

Funding: This research was supported by the Russian Science Foundation (laboratory investigations were carried out within the framework of the project No. 19-77-00016) and Tomsk Polytechnic University Competitiveness Enhancement Program (the field expeditions and sample collection).

Acknowledgments: The authors are grateful to I.P. Semiletov, the head of the Laboratory of Arctic studies of the Pacific Oceanological Institute, for the opportunity afforded to take part in field studies, and Padalko N.L., the Scientific Secretary of Siberian Research Institute of Geology, Geophysics and Mineral Resources, for help in the performance of analytical studies. The authors thank the editor and two anonymous reviewers for their constructive criticisms and revisions, which led to the improvement of the manuscript.

Conflicts of Interest: The authors declare no conflict of interest.

References

1. Buckman, J.; Donnelly, T.; Jiang, Z.; Lewis, H.; Ru, A. Methane Derived Authigenic Carbonate (MDAC) Aragonite Cemented Quaternary Hardground from a Methane Cold Seep, Rathlin Basin, Northern Ireland: δ 13 C and δ 18 O Isotopes, Environment, Porosity and Permeability. *Geosciences* **2020**, *10*, 255. [CrossRef]
2. Gabitov, R.; Borrelli, C.; Buettner, J.; Kirkland, B.; Skarke, A.; Trail, D.; Garner, B.; Testa, M.; Wahidi, M.; Hoff, C.; et al. Characterization of carbonate crust from a recently discovered methane seep on the north Atlantic continental margin of the USA. *Minerals* **2019**, *9*, 138. [CrossRef]
3. Guan, H.; Sun, Z.; Mao, S.; Xu, L.; Cao, H.; Geng, W.; Xu, C.; Zhang, X.; Wu, N. Authigenic carbonate formation revealed by lipid biomarker inventory at hydrocarbon seeps: A case study from the Okinawa Trough. *Mar. Pet. Geol.* **2019**, *101*, 502–511. [CrossRef]
4. Liang, Q.; Hu, Y.; Feng, D.; Peckmann, J.; Chen, L.; Yang, S.; Liang, J.; Tao, J.; Chen, D. Authigenic carbonates from newly discovered active cold seeps on the northwestern slope of the South China Sea: Constraints on fluid sources, formation environments, and seepage dynamics. *Deep. Res. Part I Oceanogr. Res. Pap.* **2017**, *124*, 31–41. [CrossRef]
5. Núñez-Useche, F.; Canet, C.; Liebetrau, V.; Puig, T.P.; Ponciano, A.C.; Alfonso, P.; Berndt, C.; Hensen, C.; Mortera-Gutierrez, C.; Rodríguez-Díaz, A.A. Redox conditions and authigenic mineralization related to cold seeps in central Guaymas Basin, Gulf of California. *Mar. Pet. Geol.* **2018**, *95*, 1–15. [CrossRef]
6. Peckmann, J.; Reimer, A.; Luth, U.; Luth, C.; Hansen, B.T.; Heinicke, C.; Hoefs, J.; Reitner, J. Methane-derived carbonates and authigenic pyrite from the northwestern Black Sea. *Mar. Geol.* **2001**, *177*, 129–150. [CrossRef]
7. Smith, J.P.; Coffin, R.B. Methane flux and authigenic carbonate in shallow sediments overlying methane hydrate bearing strata in Alaminos Canyon, Gulf of Mexico. *Energies* **2014**, *7*, 6118–6141. [CrossRef]

8. Shakhova, N.; Semiletov, I.; Salyuk, A.; Yusupov, V.; Kosmach, D.; Gustafsson, Ö. Extensive methane venting to the atmosphere from sediments of the East Siberian Arctic Shelf. *Science (80-.)* **2010**, *327*, 1246–1250. [CrossRef]
9. Lobkovskiy, L.I.; Nikiforov, S.L.; Dmitrevskiy, N.N.; Libina, N.V.; Semiletov, I.P.; Ananiev, R.A.; Meluzov, A.A.; Roslyakov, A.G. Mechanisms Responsible for Gas Emission and Underwater Permafrost Degradation on Laptev Sea Shelf. *Oceanology* **2015**, *55*, 312–320. [CrossRef]
10. Gresov, A.I.; Obzhirov, A.I.; Yatsuk, A.V.; Mazurov, A.K.; Ruban, A.S. Gas content of bottom sediments and geochemical indicators of oil and gas on the shelf of the East Siberian Sea. *Russ. J. Pacific Geol.* **2017**, *11*. [CrossRef]
11. Barnes, R.O.; Goldberg, E.D. Methane production and consumption in anoxic marine sediments. *Geology* **1976**, *4*, 297–300. [CrossRef]
12. Hoehler, T.M.; Alperin, M.J.; Albert, D.B.; Martens, C.S. Field and laboratory studies of methane oxidation in an anoxic marine sediment: Evidence for a methanogen-sulfate reducer consortium. *Global Biogeochem. Cycles* **1994**, *8*, 451–463. [CrossRef]
13. Naehr, T.H.; Eichhubl, P.; Orphan, V.J.; Hovland, M.; Paull, C.K.; Ussler, W.; Lorenson, T.D.; Greene, H.G. Authigenic carbonate formation at hydrocarbon seeps in continental margin sediments: A comparative study. *Deep. Res. Part II Top. Stud. Oceanogr.* **2007**, *54*, 1268–1291. [CrossRef]
14. Teichert, B.M.A.; Eisenhauer, A.; Bohrmann, G.; Haase-Schramm, A.; Bock, B.; Linke, P. U/Th systematics and ages of authigenic carbonates from Hydrate Ridge, Cascadia Margin: Recorders of fluid flow variations. *Geochim. Cosmochim. Acta* **2003**, *67*, 3845–3857. [CrossRef]
15. Birgel, D.; Feng, D.; Roberts, H.H.; Peckmann, J. Changing redox conditions at cold seeps as revealed by authigenic carbonates from Alaminos Canyon, northern Gulf of Mexico. *Chem. Geol.* **2011**, *285*, 82–96. [CrossRef]
16. Bottrell, S.H.; Newton, R.J. Reconstruction of changes in global sulfur cycling from marine sulfate isotopes. *Earth-Science Rev.* **2006**, *75*, 59–83. [CrossRef]
17. Boetius, A.; Ravenschlag, K.; Schubert, C.J.; Rickert, D.; Widdel, F.; Gleseke, A.; Amann, R.; Jørgensen, B.B.; Witte, U.; Pfannkuche, O. A marine microbial consortium apparently mediating anaerobic oxidation methane. *Nature* **2000**, *407*, 623–626. [CrossRef]
18. Lu, Y.; Liu, Y.; Sun, X.; Lin, Z.; Xu, L.; Lu, H.; Hao, X.; Peckmann, J. Intensity of methane seepage reflected by relative enrichment of heavy magnesium isotopes in authigenic carbonates: A case study from the South China Sea. *Deep. Res. Part I Oceanogr. Res. Pap.* **2017**, *129*, 10–21. [CrossRef]
19. Thiagarajan, N.; Crémière, A.; Blättler, C.; Lepland, A.; Kirsimäe, K.; Higgins, J.; Brunstad, H.; Eiler, J. Stable and clumped isotope characterization of authigenic carbonates in methane cold seep environments. *Geochim. Cosmochim. Acta* **2020**, *279*, 204–219. [CrossRef]
20. Feng, D.; Roberts, H.H.; Joye, S.B.; Heydari, E. Formation of low-magnesium calcite at cold seeps in an aragonite sea. *Terra Nov.* **2014**, *26*, 150–156. [CrossRef]
21. Xu, F.; You, X.; Li, Q.; Liu, Y. Can Primary Ferroan Dolomite and Ankerite Be Precipitated? Its Implications for Formation of Submarine Methane-Derived Authigenic Carbonate (MDAC) Chimney. *Minerals* **2019**, *9*, 413. [CrossRef]
22. Greinert, J.; Derkachev, A. Glendonites and methane-derived Mg-calcites in the Sea of Okhotsk, Eastern Siberia: Implications of a venting-related ikaite/glendonite formation. *Mar. Geol.* **2004**, *204*, 129–144. [CrossRef]
23. Bayon, G.; Dupré, S.; Ponzevera, E.; Etoubleau, J.; Chéron, S.; Pierre, C.; Mascle, J.; Boetius, A.; De Lange, G.J. Formation of carbonate chimneys in the Mediterranean Sea linked to deep-water oxygen depletion. *Nat. Geosci.* **2013**, *6*, 755–760. [CrossRef]
24. Cui, H.; Kaufman, A.J.; Xiao, S.; Zhou, C.; Liu, X.M. Was the Ediacaran Shuram Excursion a globally synchronized early diagenetic event? Insights from methane-derived authigenic carbonates in the uppermost Doushantuo Formation, South China. *Chem. Geol.* **2017**, *450*, 59–80. [CrossRef]
25. Tong, H.; Feng, D.; Cheng, H.; Yang, S.; Wang, H.; Min, A.G.; Edwards, R.L.; Chen, Z.; Chen, D. Authigenic carbonates from seeps on the northern continental slope of the South China Sea: New insights into fluid sources and geochronology. *Mar. Pet. Geol.* **2013**, *43*, 260–271. [CrossRef]

26. Mansour, A.S.; Sassen, R. Mineralogical and stable isotopic characterization of authigenic carbonate from a hydrocarbon seep site, Gulf of Mexico slope: Possible relation to crude oil degradation. *Mar. Geol.* **2011**, *281*, 59–69. [CrossRef]
27. Wang, M.; Li, Q.; Cai, F.; Liang, J.; Yan, G.; Wang, Z.; Sun, Y.; Luo, D.; Dong, G.; Cao, Y. Formation of authigenic carbonates at a methane seep site in the middle Okinawa Trough, East China Sea. *J. Asian Earth Sci.* **2019**, *185*, 104028. [CrossRef]
28. Pierre, C.; Blanc-Valleron, M.M.; Demange, J.; Boudouma, O.; Foucher, J.P.; Pape, T.; Himmler, T.; Fekete, N.; Spiess, V. Authigenic carbonates from active methane seeps offshore southwest Africa. *Geo-Marine Lett.* **2012**, *32*, 501–513. [CrossRef]
29. Botz, R.; Wehner, H.; Schmitt, M.; Worthington, T.J.; Schmidt, M.; Stoffers, P. Thermogenic hydrocarbons from the offshore Calypso hydrothermal field, Bay of Plenty, New Zealand. *Chem. Geol.* **2002**, *186*, 235–248. [CrossRef]
30. Whiticar, M.J.; Faber, E.; Schoell, M. Biogenic methane formation in marine and freshwater environments: CO2 reduction vs. acetate fermentation-Isotope evidence. *Geochim. Cosmochim. Acta* **1986**, *50*, 693–709. [CrossRef]
31. Xi, S.; Zhang, X.; Du, Z.; Li, L.; Wang, B.; Luan, Z.; Lian, C.; Yan, J. Laser Raman detection of authigenic carbonates from cold seeps at the Formosa Ridge and east of the Pear River Mouth Basin in the South China Sea. *J. Asian Earth Sci.* **2018**, *168*, 207–224. [CrossRef]
32. Peckmann, J.; Thiel, V. Carbon cycling at ancient methane-seeps. *Chem. Geol.* **2004**, *205*, 443–467. [CrossRef]
33. Sassen, R.; Sweet, S.T.; Milkov, A.V.; DeFreitas, D.A.; Kennicutt, M.C. Thermogenic vent gas and gas hydrate in the gulf of Mexico slope: Is gas hydrate decomposition significant? *Geology* **2001**, *29*, 107–110. [CrossRef]
34. Shakhova, N.; Semiletov, I.; Sergienko, V.; Lobkovsky, L.; Yusupov, V.; Salyuk, A.; Salomatin, A.; Chernykh, D.; Kosmach, D.; Panteleev, G.; et al. The East Siberian Arctic Shelf: Towards further assessment of permafrost-related methane fluxes and role of sea ice. *Philos. Trans. R. Soc. A Math. Phys. Eng. Sci.* **2015**, *373*, 20140451. [CrossRef]
35. Baranov, B.; Galkin, S.; Vedenin, A.; Dozorova, K.; Gebruk, A.; Flint, M. Methane seeps on the outer shelf of the Laptev Sea: Characteristic features, structural control, and benthic fauna. *Geo-Marine Lett.* **2020**, 1–17. [CrossRef]
36. Drachev, S.S. On the basement tectonics of the Laptev Sea shelf. *Geotectonics* **2002**, *36*, 483–497.
37. Sekretov, S.B. Structure and tectonic evolution of the Southern Eurasia Basin, Arctic Ocean. *Tectonophysics* **2002**, *351*, 193–243. [CrossRef]
38. Sergienko, V.I.; Lobkovskii, L.I.; Semiletov, I.P.; Dudarev, O.V.; Dmitrievskii, N.N.; Shakhova, N.E.; Romanovskii, N.N.; Kosmach, D.A.; Nikol'Skii, D.N.; Nikiforov, S.L.; et al. The degradation of submarine permafrost and the destruction of hydrates on the shelf of east arctic seas as a potential cause of the Methane Catastrophe: Some results of integrated studies in 2011. *Dokl. Earth Sci.* **2012**, *446*, 1132–1137. [CrossRef]
39. Romanovskii, N.N.; Hubberten, H.W.; Gavrilov, A.V.; Tumskoy, V.E.; Tipenko, G.S.; Grigoriev, M.N.; Siegert, C. Thermokarst and land-ocean interactions, Laptev Sea region, Russia. *Permafr. Periglac. Process.* **2000**, *11*, 137–152. [CrossRef]
40. Shakhova, N.; Semiletov, I. Methane release and coastal environment in the East Siberian Arctic shelf. *J. Mar. Syst.* **2007**, *66*, 227–243. [CrossRef]
41. Coplen, T.B.; Kendall, C.; Hopple, J. Comparison of stable isotope reference samples. *Nature* **1983**, *302*, 236–238. [CrossRef]
42. Díaz-del-Río, V.; Somoza, L.; Martinez-Frias, J.; Mata, M.P.; Delgado, A.; Hernandez-Molina, F.J.; Lunar, R.; Martin-Rubi, J.A.; Maestro, A.; Fernandez-Puga, M.C.; et al. Vast fields of hydrocarbon-derived carbonate chimneys related to the accretionary wedge/olistostrome of the Gulf of Cádiz. *Mar. Geol.* **2003**, *195*, 177–200. [CrossRef]
43. Magalhães, V.H.; Pinheiro, L.M.; Ivanov, M.K.; Kozlova, E.; Blinova, V.; Kolganova, J.; Vasconcelos, C.; McKenzie, J.A.; Bernasconi, S.M.; Kopf, A.J.; et al. Formation processes of methane-derived authigenic carbonates from the Gulf of Cadiz. *Sediment. Geol.* **2012**, *243–244*, 155–168. [CrossRef]
44. Dudarev, O.; Gustafsson, O.; Semiletov, I.; Jakobsson, M.; Shakhova, N.; Tesi, T.; Ruban, A.; Charkin, A. Specific features of sedimentology in the outer part of the East Siberian Arctic Shelf. In Proceedings of the AGU Fall Meeting, San Francisco, CA, USA, 14–18 December 2015; pp. C43A–0770.

45. Panova, E.V.; Ruban, A.S.; Dudarev, O.V.; Tesi, T.; Broöder, L.; Gustafsson, O.; Grinko, A.A.; Shakhova, N.E.; Goncharov, I.V.; Mazurov, A.K.; et al. Lithological features of surface sediment and their influence on organic matter distribution across the east-Siberian Arctic shelf. *Bull. Tomsk Polytech. Univ. Geo Assets Eng.* **2017**, *328*, 94–105.
46. Kravchishina, M.D.; Lein, A.Y.; Savvichev, A.S.; Reykhard, L.E.; Dara, O.M.; Flint, M.V. Authigenic Mg-calcite at a cold methane seep site in the Laptev Sea. *Oceanology* **2017**, *57*, 174–191. [CrossRef]
47. Kosmach, D.A.; Sergienko, V.I.; Dudarev, O.V.; Kurilenko, A.V.; Gustafsson, O.; Semiletov, I.P.; Shakhova, N.E. Methane in the surface waters of Northern Eurasian marginal seas. *Dokl. Chem.* **2015**, *465*, 281–285. [CrossRef]
48. Shakhova, N.; Semiletov, I.; Chuvilin, E. Understanding the Permafrost–Hydrate System and Associated Methane Releases in the East Siberian Arctic Shelf. *Geosciences* **2019**, *9*, 251. [CrossRef]
49. Li, J.; Peng, X.; Bai, S.; Chen, Z.; Van Nostrand, J.D. Biogeochemical processes controlling authigenic carbonate formation within the sediment column from the Okinawa Trough. *Geochim. Cosmochim. Acta* **2018**, *222*, 363–382. [CrossRef]
50. Berner, R.A. Sedimentary pyrite formation: An update. *Geochim. Cosmochim. Acta* **1984**, *48*, 605–615. [CrossRef]
51. Luff, R.; Greinert, J.; Wallmann, K.; Klaucke, I.; Suess, E. Simulation of long-term feedbacks from authigenic carbonate crust formation at cold vent sites. *Chem. Geol.* **2005**, *216*, 157–174. [CrossRef]
52. Treude, T.; Boetius, A.; Knittel, K.; Wallmann, K.; Jørgensen, B.B. Anaerobic oxidation of methane above gas hydrates at Hydrate Ridge, NE Pacific Ocean. *Mar. Ecol. Prog. Ser.* **2003**, *264*, 1–14. [CrossRef]
53. Ketzer, M.; Praeg, D.; Pivel, M.A.G.; Augustin, A.H.; Rodrigues, L.F.; Viana, A.R.; Cupertino, J.A. Gas seeps at the edge of the gas hydrate stability zone on Brazil's continental margin. *Geoscience* **2019**, *9*, 193. [CrossRef]
54. Luff, R.; Wallmann, K.; Aloisi, G. Numerical modeling of carbonate crust formation at cold vent sites: Significance for fluid and methane budgets and chemosynthetic biological communities. *Earth Planet. Sci. Lett.* **2004**, *221*, 337–353. [CrossRef]
55. Teichert, B.M.A.; Bohrmann, G.; Suess, E. Chemoherms on Hydrate Ridge - Unique microbially-mediated carbonate build-ups growing into the water column. *Palaeogeogr. Palaeoclimatol. Palaeoecol.* **2005**, *227*, 67–85. [CrossRef]
56. Chen, F.; Hu, Y.; Feng, D.; Zhang, X.; Cheng, S.; Cao, J.; Lu, H.; Chen, D. Evidence of intense methane seepages from molybdenum enrichments in gas hydrate-bearing sediments of the northern South China Sea. *Chem. Geol.* **2016**, *443*, 173–181. [CrossRef]
57. Nöthen, K.; Kasten, S. Reconstructing changes in seep activity by means of pore water and solid phase Sr/Ca and Mg/Ca ratios in pockmark sediments of the Northern Congo Fan. *Mar. Geol.* **2011**, *287*, 1–13. [CrossRef]
58. Himmler, T.; Birgel, D.; Bayon, G.; Pape, T.; Ge, L.; Bohrmann, G.; Peckmann, J. Formation of seep carbonates along the Makran convergent margin, northern Arabian Sea and a molecular and isotopic approach to constrain the carbon isotopic composition of parent methane. *Chem. Geol.* **2015**, *415*, 102–117. [CrossRef]
59. Merinero, R.; Lunar, R.; Martínez-Frías, J.; Somoza, L.; Díaz-del-Río, V. Iron oxyhydroxide and sulphide mineralization in hydrocarbon seep-related carbonate submarine chimneys, Gulf of Cadiz (SW Iberian Peninsula). *Mar. Pet. Geol.* **2008**, *25*, 706–713. [CrossRef]
60. Merinero, R.; Lunar, R.; Somoza, L.; Díaz-Del-Río, V.; Martínez-Frías, J. Nucleation, growth and oxidation of framboidal pyrite associated with hydrocarbon-derived submarine chimneys: Lessons learned from the Gulf of Cadiz. *Eur. J. Mineral.* **2009**, *21*, 947–961. [CrossRef]
61. González, F.J.; Somoza, L.; Lunar, R.; Martínez-Frías, J.; Rubí, J.A.M.; Torres, T.; Ortíz, J.E.; Díaz-del-Río, V. Fe-Mn nodules associated with hydrocarbon seeps: A new discovery in the Gulf of Cadiz (eastern central Atlantic). *Episodes* **2007**, *30*, 187–196. [CrossRef]
62. Franchi, F.; Rovere, M.; Gamberi, F.; Rashed, H.; Vaselli, O.; Tassi, F. Authigenic minerals from the Paola Ridge (southern Tyrrhenian Sea): Evidences of episodic methane seepage. *Mar. Pet. Geol.* **2017**, *86*, 228–247. [CrossRef]
63. Feng, D.; Chen, D.; Peckmann, J.; Bohrmann, G. Authigenic carbonates from methane seeps of the northern Congo fan: Microbial formation mechanism. *Mar. Pet. Geol.* **2010**, *27*, 748–756. [CrossRef]
64. Ye, S.; Soo, H.; Sik, M.; Xian, C. The rare earth element compositions of the Changjiang (Yangtze) and Huanghe (Yellow) river sediments. *Earth Planet. Sci. Lett.* **2002**, *201*, 407–419.

65. Hu, Y.; Chen, L.; Feng, D.; Liang, Q.; Xia, Z.; Chen, D. Geochemical record of methane seepage in authigenic carbonates and surrounding host sediments: A case study from the South China Sea. *J. Asian Earth Sci.* **2017**, *138*, 51–61. [CrossRef]
66. Miyajima, Y.; Watanabe, Y.; Goto, A.S.; Jenkins, R.G.; Sakai, S.; Matsumoto, R.; Hasegawa, T. Archael lipid biomarker as a tool to constrain the origin of methane at ancient methane seeps: Insight into subsurface fluid flow in the geological past. *J. Asian Earth Sci.* **2020**, *189*, 104134. [CrossRef]
67. Sackett, W.M. Carbon and hydrogen isotope effects during the thermocatalytic production of hydrocarbons in laboratory simulation experiments. *Geochim. Cosmochim. Acta* **1978**, *42*, 571–580. [CrossRef]
68. Greinert, J.; Bohrmann, G.; Suess, E. Gas Hydrate-Associated Carbonates and Methane-Venting at Hydrate Ridge: Classification, Distribution, and Origin of Authigenic Lithologies. In *Geophysical Monograph Series*; Blackwell Publishing Ltd.: New Jersey, NJ, USA, 2001; Vol. 124, pp. 99–113.
69. Naehr, T.H.; Rodriguez, N.M.; Bohrmann, G.; Paull, C.K.; Botz, R. Methane-derived authigenic carbonates associated with gas hydrate decomposition and fluid venting above the Blake Ridge Diapir. In *Proceedings of the Ocean Drilling Program: Scientific Results*; Texas A and M University: College Station, TX, USA, 2000; Vol. 164, pp. 285–300.
70. Grinko, A.; Goncharov, I.V.; Shakhova, N.E.; Gustafsson, Ö.; Oblasov, N.V.; Romankevich, E.A.; Zarubin, A.G.; Kashapov, R.S.; Chernykh, D.V.; Gershelis, E.V.; et al. Sediment organic matter in areas of intense methane release in the laptev sea: Characteristics of molecular composition. *Russ. Geol. Geophys.* **2020**, *61*, 456–477. [CrossRef]
71. Aharon, P.; Schwarcz, H.P.; Roberts, H.H. Radiometric dating of submarine hydrocarbon seeps in the Gulf of Mexico. *Geol. Soc. Am. Bull.* **1997**, *109*, 568–579. [CrossRef]
72. Smrzka, D.; Zwicker, J.; Misch, D.; Walkner, C.; Gier, S.; Monien, P.; Bohrmann, G.; Peckmann, J. Oil seepage and carbonate formation: A case study from the southern Gulf of Mexico. *Sedimentology* **2019**, *66*, 2318–2353. [CrossRef]
73. Roberts, H.H.; Feng, D.; Joye, S.B. Cold-seep carbonates of the middle and lower continental slope, northern Gulf of Mexico. *Deep. Res. Part II Top. Stud. Oceanogr.* **2010**, *57*, 2040–2054. [CrossRef]
74. Sun, Y.; Gong, S.; Li, N.; Peckmann, J.; Jin, M.; Roberts, H.H.; Chen, D.; Feng, D. A new approach to discern the hydrocarbon sources (oil vs. methane) of authigenic carbonates forming at marine seeps. *Mar. Pet. Geol.* **2020**, *114*, 104230. [CrossRef]
75. Anderson, T.F.; Arthur, M.A. Stable isotopes of oxygen and carbon and their application to sedimentologic and paleoenvironmental problems. *Unkn. J.* **1983**, *10*, 1.1–1.151. [CrossRef]
76. Dubinina, E.O.; Miroshnikov, A.Y.; Kossova, S.A.; Shchuka, S.A. Modification of the Laptev Sea Freshened Shelf Waters based on Isotope and Salinity Relations. *Geochemistry Int.* **2019**, *57*, 1–19. [CrossRef]